# Intermolecular interaction and cooperativity in an Fe(II) spin crossover molecular thin film system

Guanhua Hao<sup>1,2,5</sup>, Ashley S Dale<sup>3,5</sup>, Alpha T N'Diaye<sup>2,\*</sup>, Rajesh V Chopdekar<sup>2,6</sup>, Roland J Koch<sup>2,7</sup>, Xuanyuan Jiang<sup>1,8</sup>, Corbyn Mellinger<sup>1</sup>, Jian Zhang<sup>4</sup>, Ruihua Cheng<sup>3</sup>, Xiaoshan Xu<sup>1</sup> and Peter A Dowben<sup>1</sup>

- Department of Physics and Astronomy, Jorgensen Hall, University of Nebraska, Lincoln, NE 68588, United States of America
- <sup>2</sup> Advanced Light Source, Lawrence Berkeley National Lab, One Cyclotron Rd, Berkeley, CA 94720, United States of America
- <sup>3</sup> Department of Physics, Indiana University-Purdue University Indianapolis, Indianapolis, Indiana 46202, United States of America
- <sup>4</sup> The Molecular Foundry, Lawrence Berkeley National Laboratory, One Cyclotron Road, Berkeley, CA 94720, United States of America

E-mail: atndiaye@lbl.gov

Received 22 February 2022, revised 22 March 2022 Accepted for publication 4 May 2022 Published 19 May 2022



# **Abstract**

Compact domain features have been observed in spin crossover  $[Fe\{H_2B(pz)_2\}_2(bipy)]$  molecular thin film systems via soft x-ray absorption spectroscopy and photoemission electron microscopy. The domains are in a mixed spin state that on average corresponds to roughly 2/3 the high spin occupation of the pure high spin state. Monte Carlo simulations support the presence of intermolecular interactions that can be described in terms of an Ising model in which interactions beyond nearest-neighbors cannot be neglected. This suggests the presence of short-range order to permit interactions between molecules beyond nearest neighbor that contribute to the formation of largely high spin state domains structure. The formation of a spin state domain structure appears to be the result of extensive cooperative effects.

Keywords: spin crossover, PEEM, spectromicroscopy, x-ray absorption, spin crossover molecule, long range interaction, molecular thin film

(Some figures may appear in colour only in the online journal)

#### 1. Introduction

Spin crossover molecular compounds have attracted wide attention due to their potential applications [1, 2] in information technology. While bistability and low barrier for transition

- \* Author to whom any correspondence should be addressed.
- <sup>5</sup> GH and ASD have contributed equally and share first authorship.
- <sup>6</sup> Current address: Western Digital Research Center, Western Digital Corporation, San Jose, California 95119, United States of America.
- <sup>7</sup> Current address: KLA Tencor, 3 Technology Dr, Milpitas, CA 95035.
- <sup>8</sup> Current address: University of Florida, Center for Molecular Magnetic Quantum Materials, Gainesville, FL, United States of America.

of the spin state in those molecules could allow for unprecedented device efficiency, we know very little about the spatial distribution of the spin state, even in simple model systems. With spin crossover molecular compounds, the bistable nature is typically evident as hysteretic behavior in the spin state, as a function of temperature [3–9]. The nature of the spin crossover transition between the low spin (LS) state and high spin (HS) state, with bistability, is a competition between the entropy, the mean spin interaction energy and the ligand field (quantified by the ligand field parameter) [10–12]. In spin crossover molecular systems, intermolecular interaction is associated with the

so-called 'cooperative effects', bridging its microscopic and macroscopic properties [7, 13]. Cooperative effects are known to drive the hysteretic behavior (i.e. bistability) observed in thin film systems [9, 14–32].

A simple description to study an entropy-induced phase transition and other cooperative phenomena is the Ising-like model with the an activation energy for the transition between the LS and HS states, and with nearest neighbor interaction [3]. In spin crossover compounds, molecules in the HS state versus the ones in the low spin state have a difference in bond length and angles and consequently their size and geometry subtly changes upon the state switching [12, 13, 33, 34]. A transition in local spin states can cause a distortion in the lattice, and this induced elastic strain results in long-range interactions which can be expressed through an Ising-type Hamiltonian [3, 12, 13, 34–39]. On the other hand, the short-range interactions are also important and can depend on spin state, due to the fact that the potential energy function is spin-state-dependent [3, 40–42]. The phase transition and related cooperative behavior is a result of both types of interactions [13,20,43,44]. While significant long-range interactions can suppress the generation of domain structures and favor placing all molecules in the same spin state, short-range exchange interaction could favor either pairs of same spin (HS-HS, LS-LS) or pairs with different spins (HS-LS pair) [13]. In addition to Ising-type Hamiltonian models of intermolecular interactions [3, 12, 12, 34–39], models including molecular dynamics [45, 46] and Monte Carlo simulations [47, 48] have been implemented in an effort to model the spin state transition. In spite of the fact there is no free electron density and dipolar interactions are generally weak, magnetic exchange has also been suggested to play a role in the cooperativity of spin crossover systems [34, 49, 50].

This work aims to delve into the intermolecular interactions in thin films of the well-studied spin crossover molecule  $[Fe\{H_2B(pz)_2\}_2(bipy)]$ ,  $(H_2B(pz)_2 = bis(hydrido)bis(1H-pyrazol-1-yl)borate, bipy = 2,2'-bipyridine) [1, 2, 9, 12, 33, 51–57]. From the measured spin state domain structure, we can infer the presence of intermolecular interactions beyond pairwise interactions. The comparison of the experimentally determined spin state domain structure with simulation data suggests not only are nearest neighbor interactions implicated but next nearest and next-next-nearest neighbor interactions play a significant role.$ 

#### 2. Experiment methods

The spin crossover [Fe{ $H_2B(pz)_2$ }\_2(bipy)] molecule was synthesized and characterized, as noted elsewhere [2, 9, 12, 33, 51–57]. A schematic diagram of the molecule is shown in figure 1(a). [Fe{ $H_2B(pz)_2$ }\_2(bipy)] is one of the several spin crossover molecules that preserves its structure upon sublimation [9, 33, 51–57]. In this study, a nominally 15 nm thick [Fe{ $H_2B(pz)_2$ }\_2(bipy)] molecule thin film was thermally evaporated onto a 100 nm nickel cobaltate (NiCo<sub>2</sub>O<sub>4</sub>(111)) thin film, which was grown on an Al<sub>2</sub>O<sub>3</sub>(0001) substrate by pulsed laser deposition. The magnetic properties of the NiCo<sub>2</sub>O<sub>4</sub>(111) thin film have been studied systematically, as noted elsewhere

[58, 59]. For the semiconducting NiCo<sub>2</sub>O<sub>4</sub>(111) grown on Al<sub>2</sub>O<sub>3</sub>(001), ferrimagnetism occurs below  $T_c = 330$  K with a coercivity about 1000 Oe [58]. These experimentally advantageous parameters make the NiCo<sub>2</sub>O<sub>4</sub>(111)/Al<sub>2</sub>O<sub>3</sub>(001) system very suitable as a substrate for the subsequent fabrication of [Fe{H<sub>2</sub>B(pz)<sub>2</sub>}<sub>2</sub>(bipy)] thin films. Prior studies have shown that a [Fe{H<sub>2</sub>B(pz)<sub>2</sub>}<sub>2</sub>(bipy)] film on oxides [33], NiCo<sub>2</sub>O<sub>4</sub> included [53], favors occupancy of the LS state for thin films with thickness of 10 to 15 nm. This occurs for temperatures well above the spin state transition temperature of 167 K when the molecule originally favors the HS state.

The x-ray absorption spectroscopy (XAS) and x-ray photoemission electron microscopy (PEEM) measurements on [Fe{H<sub>2</sub>B(pz)<sub>2</sub>}<sub>2</sub>(bipy)] thin films were performed at the Advanced Light Source at Lawrence Berkeley National Laboratory using beamline 6.3.1 and the PEEM-3 instrument at beamline 11.0.1 [60]. The x-ray beam spot was 25 microns vertically, and about 100 microns laterally due to the grazing incidence of 30 degrees. The sample was temperature cycled between 100 K and 350 K multiple times before imaging at room temperature (297 K). Images are shown with a 16  $\mu$ m field of view.

# 3. Results and discussion

#### 3.1. Mapping of the surface spin state

X-ray PEEM has been used here to probe the two-dimensional spin state domain structure across the thin film. Figure 1 presents a PEEM image of a 15 nm [Fe{ $H_2B(pz)_2$ }\_2(bipy)] thin film on top of NiCo<sub>2</sub>O<sub>4</sub>. X-ray absorption spectra (XAS) are derived from PEEM image stacks acquired with energy steps of 0.1 eV across the Fe L<sub>2,3</sub> absorption edges. This probes transitions between the core level states and empty valence states. It is not only element specific but also sensitive to the chemical environment and molecular spin state [12, 33, 51–53, 55–57, 61, 62]. While x-ray PEEM is commonly used to image structural and magnetic domains [60, 63], we are using spectromicroscopy to derive a map of the spin states across the film surface.

At each photon energy point, an image was acquired and the images are combined in a stack where each 'pixel' is an absorption spectrum of the Fe  $L_{3,2}$  edges. The pre-edge image (at 700 eV imaging x-ray energy) is shown in figure 1(b).

The PEEM image, figure 1(b), exhibits considerable heterogeneity. While the interpretation of intensity variations on the basis of a single x-ray energy would remain ambiguous, the spin state can be determined from spectroscopic data. The spectra in figure 1(c) are derived by integrating pixel intensities over the areas marked by circles in figure 1(b) for each energy in the image stack. XAS and near-edge x-ray absorption fine structure (NEXAFS) have been shown to directly provide distinct signatures of the LS state and the HS state of Fe (II) spin crossover molecular compounds [9, 12, 33, 51–53, 55–57, 61, 62] They are a facile means for assessing the fraction of the HS state and the LS state. The HS and LS state fraction can be extracted from the XAS spectra by interpolating peak ratios of the L3 sub-peaks between 705 eV and 715 eV with those of

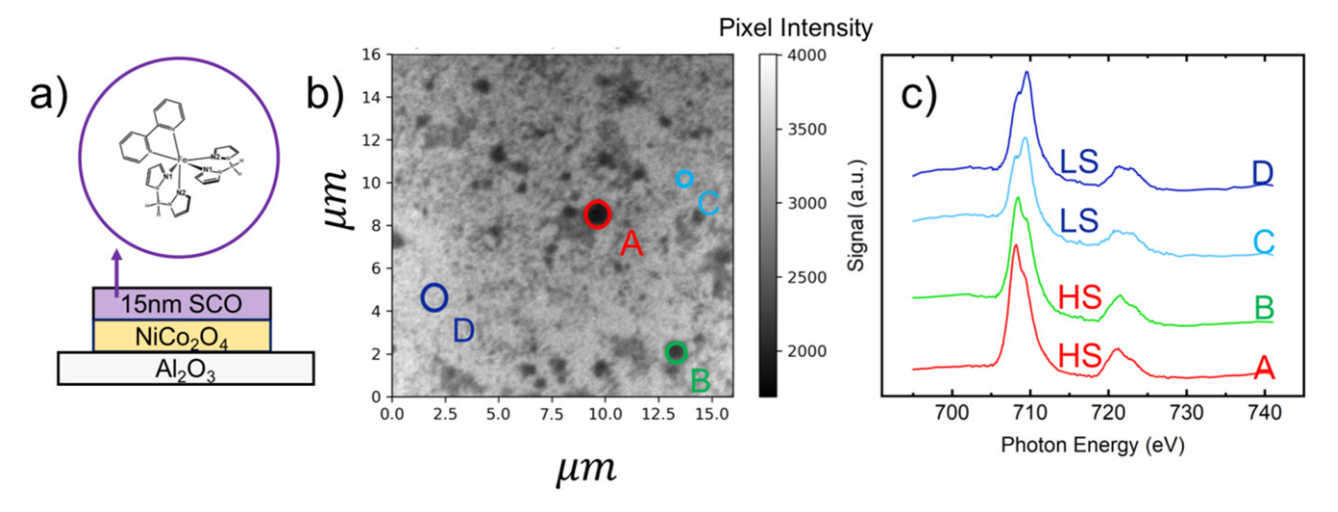


Figure 1. (a) The schematic drawing of the spin crossover molecule  $[Fe\{H_2B(pz)_2\}_2(bipy)]$  and thin film on  $NiCo_2O_4$  substrate. SCO stands for spin crossover molecule. (b) The pre-edge (700 eV) x-ray PEEM image for 15 nm of  $[Fe\{H_2B(pz)_2\}_2(bipy)]$  thin film on top of  $NiCo_2O_4$ , showing compact grain features (A, B) around seas of the flat region (C, D). (c) The Fe L3,2 edge x-ray absorption spectra for the marked area, indicating the grain features where the high spin (HS) state or low spin (LS) state for is more dominant (although not 100%).

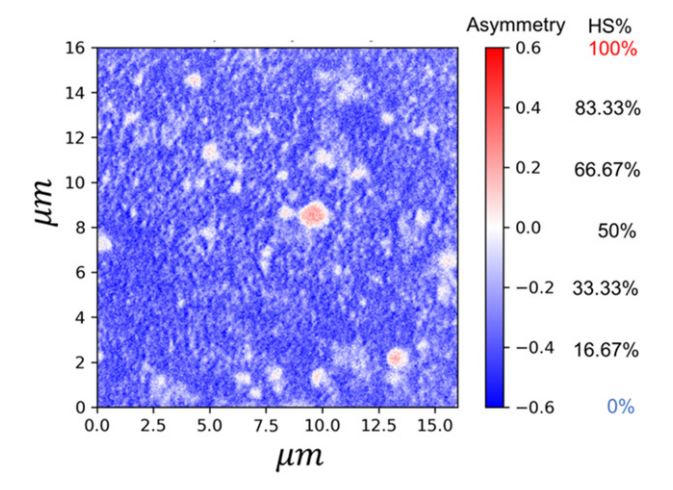
measured in benchmark spectra for the pure high-spin and pure low-spin states: in the LS state of [Fe{ $H_2B(pz)_2$ }\_2(bipy)], well below 160 K [9, 12, 33, 51–53, 55–57, 61, 62], the 3d electrons occupy the  $t_{2g}$  orbitals in pairs and the  $e_g$  orbitals are empty. This is generally observed in the Fe L<sub>3</sub> edge  $(2p_{3/2})$  XAS as a major feature at photon energy around 708 eV. By comparison, in the HS configuration, the  $e_g$  orbitals are partially populated while the  $t_{2g}$  orbitals subsequently become partly depopulated, which corresponds to the XAS spectra with a decreasing intensity of the peak at 708 eV and an increase of the  $t_{2g}$  peak around 706.5 eV. The spectra of the LS state and the HS state from the temperature dependent spin crossover transitions are good 'fingerprints' of the spin states, and can be used to infer the percentage of HS and LS state occupancy.

Figure 1(c) presents the characteristic XAS spectra of the various dominantly HS state and LS state regions of the spin crossover thin film  $[Fe\{H_2B(pz)_2\}_2(bipy)]$  on  $NiCo_2O_4(111)$ . Regions A and B denote grain-like features of the thin film while regions C and D represent more homogeneous parts of the thin film with flat contrast. The Fe L<sub>3</sub> NEXAFS in figure 1(c) reveals the fact that spectra A and B correspond to the HS state of the  $[Fe\{H_2B(pz)_2\}_2(bipy)]$  molecule, and spectra C and D correspond to the LS state. This indicates that molecules in the grain-like regions on the thin film tend to have an overall higher spin state occupation compared to their flat domain counterparts.

The asymmetry A of  $t_{2g}$  and  $e_g$  peak at  $L_3$  edge is a good indicator of the HS occupation, and can be expressed as:

$$A = rac{h_{t_{2g}} - h_{e_g}}{h_{t_{2g}} + h_{e_g}}.$$

The peak intensities  $h_{t2g}$  and  $h_{eg}$  indicative of the  $t_{2g}$  and  $t_{eg}$  unoccupied states have been determined by fitting the spectrum at the Fe-L<sub>3</sub> edge spectrum at a given pixel with two Lorentz peaks after linear background subtraction. We have extracted the asymmetry mapping of the  $[Fe\{H_2B(pz)_2\}_2(bipy)]$  thin film based on the PEEM data;



**Figure 2.** The extracted peak asymmetry map of the 15 nm thick  $[Fe\{H_2B(pz)_2\}_2(bipy)]$  thin film on  $NiCo_2O_4$ , with corresponding high spin (HS%) occupancy. The majority of the film is in the LS state, while HS grains with fraction around 2/3 to the fully HS state has been observed.

the result is presented in figure 2. Conversion of asymmetry to the percentage of material in the HS state (HS%) has been done by scaling to reference spectra obtained from  $[Fe\{H_2B(pz)_2\}_2(bipy)]$  thin films residing in pure LS and pure HS.

From the mapping result, it is clear that the majority of the thin film is in the LS state (blue), which corresponds to the flat region of the thin film. Closer to the HS state domain features, the spin state occupancy rises, with HS state dominant near the center of the grains. It should be noted that in the spin state mapping data shown in figure 2, the HS state domains (red) are not close to 100% HS state occupancy, but rather high-spin and low-spin states are mixed in a 2:1 ratio. A single molecule can only be in the definite HS state or LS state. The separation of the film into areas of pure LS state and areas that exhibit the 2:1 spin state ratio points to the formation of

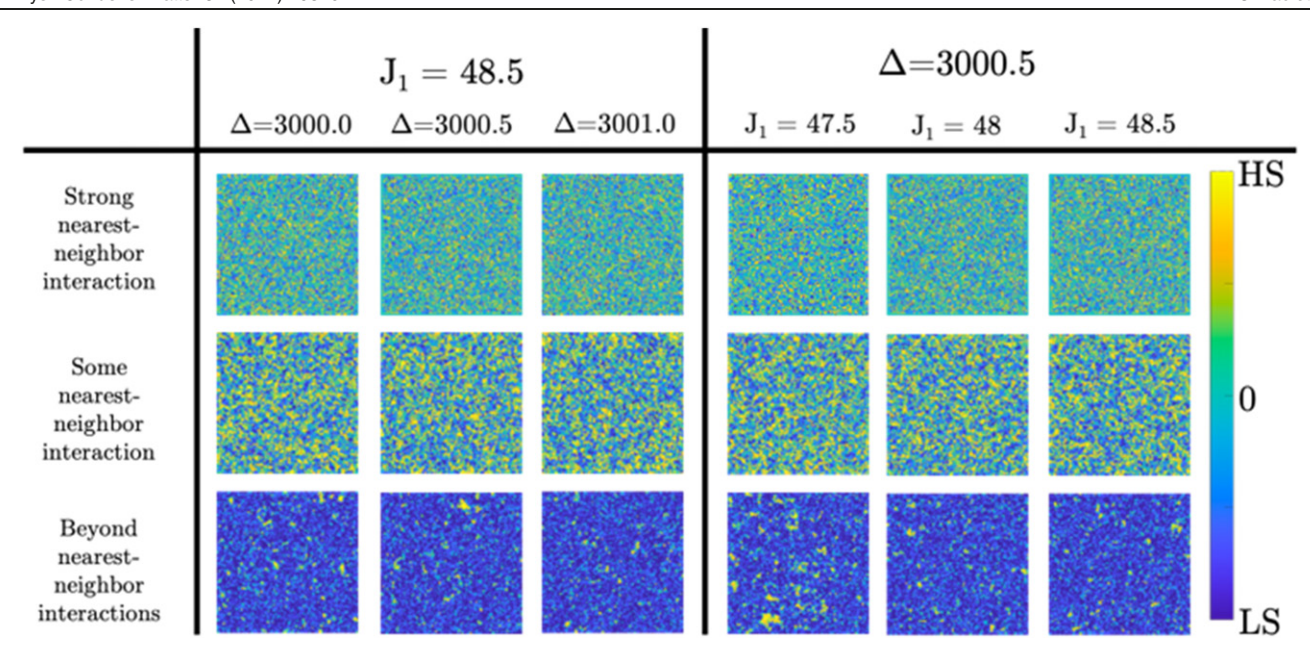


Figure 3. The Monte Carlo Ising model simulation lattice results corresponding to various interaction parameter strength and length. The infinite decay rate corresponding to  $N_1$  is shown in the row 'strong nearest-neighbor interaction', the quadratic decay rate for  $N_3$  is shown in the row 'some nearest-neighbor interaction', and the linear decay rate for  $N_3$  is shown in the row 'beyond nearest-neighbor interactions'. The linear decay in interaction length gives rise to compact HS dominated domains as seen in the experimental PEEM image.

triplets of two spin crossover molecules in the HS state and one in the LS state. Clusters with the composition of a molecular triplet (2 HS and 1 LS or 2 LS and 1 HS) seem to be energetically preferred over arbitrary spin state ratios. The presence of clusters with this particular packing reveals that cooperative effects dominate the formation of domains to reduce overall free energy.

# 3.2. Monte Carlo simulation of the domain feature

The PEEM image in figure 1(b) shows compact, circular HS dominated domains surrounded by uniformly distributed LS and mixed spin state domains. We have performed simulations have to determine what conditions lead to this domain structure. Previous studies [18, 57] have successfully employed the Ising-like Hamiltonian to represent the spin crossover system:

$$H = -J_1 \sum_{\langle N_1 \rangle} \sigma_i \sigma_j - J_2 \sum_{\langle N_2 \rangle} \sigma_i \sigma_k - J_3 \sum_{\langle N_3 \rangle} \sigma_i \sigma_l + \mu \sum_i \sigma_i$$

where J is the interaction parameter and  $\sigma$  is the fictitious spin operator taking values  $\pm 1$ . We consider the film to be thin enough for the spin state to vary only very little over its thickness of 15 nm. For this work, we assigned the LS state to the  $-1\sigma$  operator value and the 2/3 HS triplet state to the  $+1\sigma$  operator value as the PEEM data does not exhibit a fully HS domain. We also considered the sum over the next-nearest neighbor  $N_2$  and next-next-nearest neighbor  $N_3$  interactions in addition to the nearest neighbor  $N_1$  interactions on a square lattice for a total of 12 neighbors considered. The fourth term refers to the mean field term:

$$\mu = \left(\frac{\Delta}{2} - \frac{k_{\rm b}T}{2}\ln(g)\right),\,$$

where T is temperature,  $\Delta$  is the energy difference between the HS and LS states,  $k_b$  is the Boltzmann constant, and  $\ln(g)$  is the degeneracy ratio between the HS and LS states.

Next, we consider the unitless ratios of interaction parameters  $R' = J_2/J_1$  and  $R'' = J_3/J_1$  and impose a decay relation between them:

$$R(N_k) = \alpha(r_{\langle i,j\rangle})^{-n},$$

where  $r_{\langle i,j\rangle}$  is the distance between kth-order neighbors in neighborhood  $N_k$  on the square unit lattice and  $\alpha$  carries the units

We then let  $R' = R(N_2)$  and  $R'' = R(N_3)$ . Three cases for R were considered: the first of these three models considers strong nearest-neighbor interaction, yielding an infinitely steep decay  $(n = \infty)$  in interaction strength between the ith site and neighbors in  $N_2$ ,  $N_3$  such that R' = R'' = 0; this is equivalent to the commonly considered nearest-neighbors  $N_1$  interactions. The second case brings some nearest-neighbor interaction, yielding a quadratic decay  $1/r^2$  with constants R' = 1/2 and R'' = 1/4. The third case considers interactions beyond nearest-neighbors, yielding a linear decay 1/r such that  $R' = 1/\sqrt{2}$  and R'' = 1/2. For each decay rate we can determine a maximum effective coupling value:  $J_{\infty} = 1.000J_1$ ,  $J_{quadratic} = 1.750J_1$ , and  $J_{linear} = 2.207J_1$ .

A Monte Carlo Ising model simulation using the metropolis algorithm [64] was implemented with the goal of determining conditions that lead to the domain structures observed in the PEEM image in figure 1: a compact, HS domain with smooth edges surrounded by predominantly LS/mixed state background. Our simulations used a 300 by 300 square lattice with periodic boundary conditions, and experimental values T = 297 K,  $\ln(g) = S/\rho$  where  $S = 83.9 \text{ J mol}^{-1} \text{ K}^{-1}$  [65] and  $\rho$  is the gas constant  $8.314 \text{ J mol}^{-1} \text{ K}^{-1}$  with free parameters  $\Delta$ 

and  $J_1$ . To study the effect of increased cooperativity between neighbors, first a physically plausible background with  $\sim 1/3$  HS state, thus matching experiment, was achieved by letting a pure LS state evolve using nearest-neighbor  $N_1$  coupling, then the cooperativity was increased through the order of the neighborhood and the R' ratios until domains appeared. To interpolate lattice values between 0 and 1, the lattice was then downsampled by averaging over a 3 by 3 pixel neighborhood. The downsampled results of the selected simulations are presented in figure 3 for best-fit parameters  $J_1 = [47.5, 48, 48.5]$  K and  $\Delta = [3000.0, 3000.5, 3001.0]$  K.

To determine which simulation results are most comparable to the experimental results, the background was removed from both the PEEM and simulated data with an adaptive threshold so that only domain structure remained. The simulated data was interpolated to contain the same number of points as the experimental PEEM data. The results were then compared using the structural similarity (SSIM) index [66] with a default Gaussian kernel size of 11 by 11 and SSIM radius of 1.5. The SSIM index compares the local means and variances for a neighborhood of pixels within each of the two images and is therefore a metric for comparing domain shape [66]. For each set of parameters we compared ten simulations to the experimental data to obtain the corresponding SSIM index on an absolute scale of 0 to 1.

To observe high degrees of SSIM, beyond nearest-neighbor interactions need to be included in the simulation. Figure 4 shows SSIM indices between experimental data and simulations obtained with varying ranges of interaction. Linear decay simulation results reaching beyond next-next-nearest neighbors achieve a SSIM index around 0.64 (0.6354  $\pm$  0.0063 for  $J=47.5~\rm K$ , 0.6511  $\pm$  0.0057 for  $J=48~\rm K$ , and 0.6646  $\pm$  0.0063 for  $J=48.5~\rm K$ ) in relation to experimental PEEM data. Limiting the interaction range to next-next-nearest neighbors or less leads to SSIM indices around 0.35 or below 0.1 for independent thermally activated spins. We therefore conclude that these longer range cooperative effects need to be included to capture the relevant physics of this spin crossover system.

Typical Monte Carlo Ising model simulations consider only the four nearest-neighbors and a mean field term in the Hamiltonian; the nearest-neighbors represent the short range interactions and the mean field represents the long range interactions. At the critical temperature and above, these typical Monte Carlo Ising model simulations develop uniformly distributed domains with irregular borders [68]. Nakada et al further showed that implementing a crossover from short-range to long-range interactions in the Hamiltonian does not affect the uniform distribution of domains or the cluster size [68], with the implication that interaction length alone cannot account for the observed domain structure in figure 2. As shown in figure 3, we find that compact minority-state domains arise due to increased interaction (cooperativity) between adjacent lattice sites when the interaction term J decays linearly as a function of distance over the twelve nearest-neighbors.

In the spin crossover Hamiltonian, the mean field term arises from the elastic interactions that cause lattice distortion and has an infinite interaction length [67] while the short-range

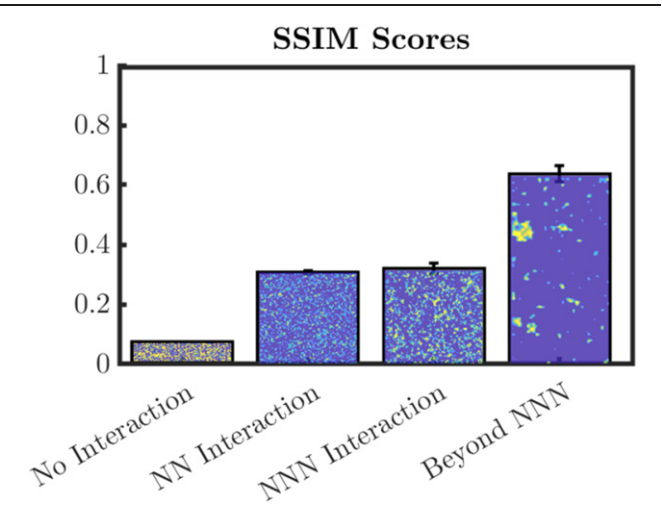


**Figure 4.** Structural similarity indices between measured domain distribution data and simulation results with different interaction length scales. Areas patterns in bars represent typical HS domain distributions from the respective simulations (color bar as in figure 3).

terms containing  $J_{1,2,3}$  correlate with intermolecular interactions and have a finite interaction length dependent on the size of the neighborhood. Binder and Landau showed the importance of the ratio between interactions of higher-order neighbors in critical point behavior and phase transitions [68, 69], while Nicolazzi et al included a Lennard-Jones potential in the spin crossover Hamiltonian to demonstrate the effect of distance on spin crossover intermolecular interactions [40]. Here, we report a lower bound of  $N_3$  for the short-range interaction length and a linear decay in interaction strength as a function of distance. Restricting the neighborhood to  $N_2$  with these constants did not yield the desired results. These results agree with Nicolazzi's description of a distance-dependent anharmonic model for SCO intermolecular interactions [40]. Although these simulation results cannot be directly mapped onto experimental results, particularly since we consider a square lattice and the simulated value of the interaction parameter  $J_1$  is a gross estimate of the undetermined experimental value [40] our findings suggest that in addition to interaction beyond nearest-neighbor interactions, the compact domain shape arises from electrostatic-like interactions.

It is possible to improve the SSIM index result by changing the scale of the simulation and forcing a larger domain size with respect to the final image (as seen in figure S1 (https://stacks.iop.org/JPCM/34/295201/mmedia) in the supplementary information with the 72 by 72 size lattice), but this has been avoided to not misrepresent the clustering for an effectively infinite lattice. The simulations are also agnostic to any effect that morphological inhomogeneities may have on the nucleation or pinning of spin crossover domains.

#### 4. Conclusions

We have observed of spin state domains in a  $[Fe\{H_2B(pz)_2\}_2(bipy)]$  spin crossover molecular thin film. We find that the film separates into domains that favor

LS state, or a mixed spin state with HS occupation around 2/3 relative to the pure HS state, and this is evident in x-ray PEEM spectromicroscopy. There are domains residing largely in the HS state that are highly compact. Corresponding Monte Carlo simulations support the presence of beyond nearest-neighbor interactions and the role these interactions play in governing the formation of domain structures with the observed compact shape. Simulations limited to nearest-neighbor interactions in SCO thin film are insufficient to explain the domain structure. Only by including beyond nearest-neighbor interactions does it become possible to reproduce the experimentally observed domain structures with the Monte Carlo simulation of this model. This work shows that nearest neighbor, next-nearest and next-next-nearest neighbor interactions all play a significant role in establishing cooperative effects. This extensive interaction beyond nearest neighbor is compelling evidence for cooperative effects in  $[Fe\{H_2B(pz)_2\}_2(bipy)]$  SCO thin films that have been indicated in compact HS state domain structures shown here and suggested by the evidence for cooperative effect previously discussed elsewhere [9].

## **Acknowledgments**

This research was supported by the National Science Foundation through NSF-DMR 2003057 [G Hao, A Dale, R Cheng, P A Dowben] and EPSCoR RII Track-1: Emergent Quantum Materials and Technologies (EQUATE), Award OIA-2044049 [X Jiang, X Xu,]. Use of the Advanced Light Source, Lawrence Berkeley National Laboratory, was supported by the US Department of Energy (DOE) under contract no. DE-AC02-05CH11231.

# Data availability statement

The data that support the findings of this study are available upon reasonable request from the authors.

#### **Author contributions**

Measurements (GH, ATN, RVC, RJK), simulations (ASD, RC), sample preparation (XJ, CM, XX), data analysis (GH, ATN, ASD, PAD), manuscript preparation (ASD, ATN, PAD).

## **Conflict of interest**

There are no conflicts to declare.

#### **ORCID iDs**

Guanhua Hao https://orcid.org/0000-0003-3281-6816
Ashley S Dale https://orcid.org/0000-0001-8233-5258
Alpha T N'Diaye https://orcid.org/0000-0001-9429-9776
Rajesh V Chopdekar https://orcid.org/0000-0001-6727-6501

Xuanyuan Jiang https://orcid.org/0000-0002-2960-0101
Corbyn Mellinger https://orcid.org/0000-0001-7587-6240
Jian Zhang https://orcid.org/0000-0003-0274-0814
Ruihua Cheng https://orcid.org/0000-0003-1579-8097
Xiaoshan Xu https://orcid.org/0000-0002-4363-392X
Peter A Dowben https://orcid.org/0000-0002-2198-4710

#### References

- [1] Ekanayaka T K et al 2021 Magnetochemistry 7 37
- [2] Hao G, Cheng R and Dowben P A 2020 J. Phys.: Condens. Matter 32 234002
- [3] Nishino M and Miyashita S 2013 Phys. Rev. B 88 014108
- [4] Cambi L and Szegö L 1931 Berichte der Dtsch Chem. Ges. A/B 64 2591–8
- [5] Hauser A 1991 Coord. Chem. Rev. 111 275-90
- [6] Gütlich P, Gaspar A B and Garcia Y 2013 Beilstein J. Org. Chem. 9 342–91
- [7] Fert A 2008 Angew. Chem., Int. Ed. 47 5956-67
- [8] Miyamachi T et al 2012 Nat. Commun. 3 938
- [9] Jiang X et al 2019 J. Phys.: Condens. Matter 31 315401
- [10] Kepp K P 2016 Inorg. Chem. 55 2717-27
- [11] Ronayne K L et al 2006 Phys. Chem. Chem. Phys. **8** 4685–93
- [12] Kipgen L et al 2018 Nat. Commun. 9 2984
- [13] Nesterov A I, Orlov Y S, Ovchinnikov S G and Nikolaev S V 2017 Phys. Rev. B 96 1–11
- [14] Bousseksou A, Molnár G, Salmon L and Nicolazzi W 2011 Chem. Soc. Rev. 40 3313
- [15] Enachescu C, Nishino M, Miyashita S, Stoleriu L and Stancu A 2012 Phys. Rev. B 86 054114
- [16] Muraoka A, Boukheddaden K, Linarès J and Varret F 2011 Phys. Rev. B 84 054119
- [17] Gütlich P and Goodwin H A (ed) 2004 Spin Crossover in Transition Metal Compounds I (Berlin: Springer)
- [18] Ekanayaka T K et al 2021 Mater. Adv. 2 760-8
- [19] Lochenie C, Schötz K, Panzer F, Kurz H, Maier B, Puchtler F, Agarwal S, Köhler A and Weber B 2018 J. Am. Chem. Soc. 140 700-9
- [20] Lochenie C, Bauer W, Railliet A P, Schlamp S, Garcia Y and Weber B 2014 *Inorg. Chem.* 53 11563–72
- [21] Lochenie C, Heinz J, Milius W and Weber B 2015 *Dalton Trans*. 44 18065–77
- [22] Bauer W, Schlamp S and Weber B 2012 Chem. Commun. 48 10222-4
- [23] Prins F, Monrabal-Capilla M, Osorio E A, Coronado E and van der Zant H S J 2011 *Adv. Mater.* **23** 1545–9
- [24] Ossinger S, Näther C, Buchholz A, Schmidtmann M, Mangelsen S, Beckhaus R, Plass W and Tuczek F 2020 *Inorg. Chem.* 59 7966–79
- [25] Gütlich P, Garcia Y and Goodwin H A 2000 Chem. Soc. Rev. 29 419–27
- [26] Mallah T and Cavallini M 2018 C. R. Chim. 21 1270-86
- [27] Gu"tlich P and Goodwin H A 2004 Spin Crossover in Transition Metal Compounds II (Berlin: Springer)
- [28] Weber B, Bauer W and Obel J 2008 Angew. Chem., Int. Ed. 47 10098–101
- [29] Real J A, Gaspar A B and Muñoz M C 2005 Dalton Trans. 2062
- [30] Bousseksou A, Molnár G, Demont P and Menegotto J 2003 J. Mater. Chem. 13 2069–71
- [31] Linares J, Nasser J, Boukheddaden K, Bousseksou A and Varret F 1995 J. Magn. Magn. Mater. 140–144 1507–8
- [32] Konishi Y, Tokoro H, Nishino M and Miyashita S 2008 Phys. Rev. Lett. 100 067206

- [33] Zhang X et al 2017 Adv. Mater. 29 1702257
- [34] Jeschke H O, Andrea Salguero L, Rahaman B, Buchsbaum C, Pashchenko V, Schmidt M U, Saha-Dasgupta T and Valentí R 2007 New J. Phys. 9 448
- [35] Zimmermann R and König E 1977 J. Phys. Chem. Solids 38 779–88
- [36] Ohnishi S and Sugano S 1981 J. Phys. C: Solid State Phys. 14 39-55
- [37] Spiering H, Meissner E, Köppen H, Müller E W and Gütlich P 1982 *Chem. Phys.* **68** 65–71
- [38] Adler P, Wiehl L, Meibner E, Köhler C P, Spiering H and Gütlich P 1987 J. Phys. Chem. Solids 48 517–25
- [39] Willenbacher N and Spiering H 1988 J. Phys. C: Solid State Phys. 21 1423–39
- [40] Nicolazzi W, Pillet S and Lecomte C 2008 Phys. Rev. B 78 174401
- [41] Nicolazzi W and Pillet S 2012 Phys. Rev. B 85 094101
- [42] Slimani A, Boukheddaden K, Varret F, Oubouchou H, Nishino M and Miyashita S 2013 Phys. Rev. B 87 014111
- [43] Pluis B, Taylor T N, Frenkel D and van der Veen J F 1989 Phys. Rev. B 40 1353–6
- [44] Giuliani A, Lebowitz J L and Lieb E H 2006 Phys. Rev. B 74 064420
- [45] Boukheddaden K, Nishino M and Miyashita S 2008 Phys. Rev. Lett. 100 177206
- [46] Nishino M, Boukheddaden K, Konishi Y and Miyashita S 2007 Phys. Rev. Lett. 98 247203
- [47] Konishi Y, Tokoro H, Nishino M and Miyashita S 2008 Phys. Rev. Lett. 100 067206
- [48] Miyashita S, Konishi Y, Nishino M, Tokoro H and Rikvold P A 2008 Phys. Rev. B 77 014105
- [49] Timm C and Schollwöck U 2005 Phys. Rev. B 71 224414
- [50] Timm C 2006 Phys. Rev. B 73 014423
- [51] Costa P et al 2018 J. Phys.: Condens. Matter 30 305503

- [52] Hao G et al 2019 Appl. Phys. Lett. 114 032901
- [53] Zhang X, N'Diaye A T, Jiang X, Zhang X, Yin Y, Chen X, Hong X, Xu X and Dowben P A 2018 Chem. Commun. 54 944–7
- [54] Palamarciuc T, Oberg J C, El Hallak F, Hirjibehedin C F, Serri M, Heutz S, Létard J-F and Rosa P 2012 J. Mater. Chem. 22 9690
- [55] Zhang X et al 2015 J. Phys. Chem. C 119 16293-302
- [56] Warner B et al 2013 J. Phys. Chem. Lett. 4 1546-52
- [57] Mosey A, Dale A S, Hao G, N'Diaye A, Dowben P A and Cheng R 2020 J. Phys. Chem. Lett. 11 8231-7
- [58] Zhen C, Zhang X, Wei W, Guo W, Pant A, Xu X, Shen J, Ma L and Hou D 2018 J. Phys. D: Appl. Phys. 51 145308
- [59] Mellinger C, Waybright J, Zhang X, Schmidt C and Xu X 2020 Phys. Rev. B 101 014413
- [60] Scholl A 2003 Curr. Opin. Solid State Mater. Sci. 7 59-66
- [61] Kipgen L et al 2017 J. Phys.: Condens. Matter 29 394003
- [62] Zhang X, N'Diaye A T, Jiang X, Zhang X, Yin Y, Chen X, Hong X, Xu X and Dowben P A 2018 Chem. Commun. 54 944-7
- [63] Baumgarten L 2012 43rd IFF Spring School: scattering methods for condensed matter research: towards novel applications at future sources Schriften des Forschungszentrums Jülich/Reihe Schlüsseltechnologien/Key Tech ed M Angst, T Brückel, D Richter and R Zorn vol 33 (Jülich: Forschungszentrum Jülich) pp 1–37
- [64] Chib S and Greenberg E 1995 Am. Stat. 49 327–35
- [65] Real J A, Muñoz M C, Faus J and Solans X 1997 *Inorg. Chem.* 36 3008–13
- [66] Wang Z, Bovik A C, Sheikh H R and Simoncelli E P 2004 IEEE Trans. Image Process. 13 600–12
- [67] Nakada T, Rikvold P A, Mori T, Nishino M and Miyashita S 2011 Phys. Rev. B 84 054433
- [68] Binder K and Landau D P 1980 Phys. Rev. B 21 1941-62
- [69] Landau D P and Binder K 1985 Phys. Rev. B 31 5946-53